Lattice Boltzmann model of immiscible fluids

Article *in* Physical Review A · May 1991

DOI: 10.1103/PhysRevA.43.4320 · Source: PubMed

4 authors, including:

Gianluigi Zanetti
CRS4 Centro di Ricerca, Sviluppo e Studi Superiori in Sardegna
147 PUBLICATIONS **6,201** CITATIONS

PHYSICAL REVIEW A VOLUME 43, NUMBER 8 15 APRIL 1991

Lattice Boltzmann model of immiscible fluids

Andrew K. Gunstensen and Daniel H. Rothman
Department of Earth, Atmospheric, and Planetary Sciences, Massachusetts Institute of Technology, Cambridge, Massachusetts 01239

Stéphane Zaleski
Laboratoire de Physique Statistique, Ecole Normale Supérieure, 24 rue Lhomond, 75321 Paris CEDEX 05, France

Gianluigi Zanetti
Program in Computational and Applied Mathematics, Princeton University, Princeton, New Jersey 08544
(Received 29 October 1990; revised manuscript received 14 January 1991)

We introduce a lattice Boltzmann model for simulating immiscible binary fluids in two dimensions. The model, based on the Boltzmann equation of lattice-gas hydrodynamics, incorporates features of a previously introduced discrete immiscible lattice-gas model. A theoretical value of the surface-tension coefficient is derived and found to be in excellent agreement with values obtained from simulations. The model serves as a numerical method for the simulation of immiscible two-phase flow; a preliminary application illustrates a simulation of flow in a two-dimensional microscopic model of a porous medium. Extension of the model to three dimensions appears straightforward.

INTRODUCTION

Discrete models of hydrodynamics known as lattice gases were recently introduced by Frisch, Hasslacher, and Pomeau (FHP).[1] In their original formulation, the lattice gas consists of a collection of discrete particles of unit mass and unit momentum moving on a triangular lattice. When particles meet at a lattice site, they collide with each other such that mass and momentum are locally conserved. At a macroscopic scale, the behavior of the lattice gas is very close to the incompressible Navier-Stokes equations.[2–5]

In addition to its intrinsic interest as a model of hydrodynamics, the lattice gas is also a useful numerical method for the simulation of complex hydrodynamic flows. Examples in the current literature include external flows in three dimensions,[6] flows in microscopic models of porous media,[7] and flows of immiscible mixtures.[8–11] In each of these areas of application, the emphasis is on the efficient simulation of gross features of the flow. Thus any small-scale inaccuracies in the lattice-gas method are potentially outweighed by its efficiency, or, indeed, its ability to simulate certain complex flows not easily accessible by other methods.

However, lattice-gas models are not free of problems. Two of the most serious disadvantages are the difficulty of extending the models, particularly the multiphase models, from two to three dimensions,[12,13] and, for many applications, the high level of statistical noise in the model. To eliminate or reduce these two problems, as well as gain insight into the workings of lattice-gas models, two related adaptations of the lattice-gas model, known as *lattice Boltzmann* models, have been introduced.[14,15] The first version is an explicit solution of the Boltzmann equation that is obtained by assuming that there are no correlations between particles.[14] Probabilities or, equivalently, average populations, substitute for discrete particles, and each Boolean FHP collision is expressed as an arithmetic nonlinear collision operator in the resulting Boltzmann equation. In the second version of a lattice Boltzmann model, the nonlinear collision operator is linearized about a local equilibrium.[15,16] Both lattice Boltzmann models retain the original macroscopic adherence to the Navier-Stokes equations. In addition, both models are free of statistical noise. However, only the second of these two approaches is easily implemented in three dimensions.

Lattice Boltzmann models have thus far only been introduced for the simulation of single-species fluids. Thus, one of the most promising applications of lattice-gas methods—the simulation of immiscible two-phase flows—has not yet been approachable with the advantages of the lattice Boltzmann method. Our objective in this paper, therefore, is to introduce a method that not only retains the advantages of the lattice Boltzmann approach but also provides the ability to simulate complex multiphase flows.

Specifically, our model is a variant of both the lattice Boltzmann model of Refs. 15 and 16 and the immiscible lattice-gas model of Ref. 8. In a two-species version of a lattice Boltzmann model, we add a perturbation to the linearized collision operator that makes the pressure tensor locally anisotropic near a fluid-fluid interface. This addition results in surface tension at interfaces while retaining the adherence to the Navier-Stokes equations in homogeneous regions. Though capable of general applications, we expect that our model's greatest utility will be for the simulation of immiscible two-phase flow in microscopic models of three-dimensional (3D) porous media.

The paper proceeds as follows. We first formulate a Galilean-invariant, linearized collision operator by combining ideas previously presented in Refs. 15–17. The perturbation scheme that provides for surface tension is

then developed in detail. From this scheme, a theoretical prediction of the surface-tension coefficient is derived. This theoretical prediction is then compared with three independent surface-tension measurements obtained from numerical simulation of the model. In all cases, good agreement between simulation and theory is obtained. Finally, a preliminary application of the model is demonstrated with a simulation of immiscible two-phase flow in a microscopic model of a porous medium.

SINGLE-PHASE LATTICE BOLTZMANN COLLISION OPERATOR

The FHP lattice gas models the fluid as a collection of identical particles, each of unit mass and momentum, moving on a triangular lattice. At nodes of the lattice the particles collide with other particles present at the node, redistributing the particles among the available lattice directions while conserving total mass and momentum at the node.

The particles in a FHP lattice gas can be considered as a Boolean field $n_i(\mathbf{x},t)$ where n_i is set to 1 or 0 to indicate the presence or absence of a particle with velocity $\mathbf{c}_i$ at site $\mathbf{x}$. The evolution of the system can be written as

$$n_i(\mathbf{x}+\mathbf{c}_i,t+1)=n_i(\mathbf{x},t)+\Delta_i(n)\ , \tag{1}$$

where $\mathbf{c}_i=(\cos(i-1)\pi/3,\sin(i-1)\pi/3)$ is the velocity associated with lattice direction i and $\Delta_i(n)$ is a collision operator describing the change in n_i due to a collision with other particles present at site $\mathbf{x}$. Figure 1 shows an example of a collision in the FHP model, where three particles with zero total momentum collide and change direction by 60°. For this collision, Δ_1 is given by

$$\Delta_1(n)=n_2\wedge n_4\wedge n_6\wedge\neg n_1\wedge\neg n_3\wedge\neg n_5\ , \tag{2}$$

where $\wedge$ and $\neg$ represent the AND and NOT Boolean operators, respectively. The rest of the FHP collisions contribute terms similar to this one. By adding the contributions from all collisions included in the model the collision operator $\Delta(n)$ is constructed.

The Boolean field $n_i(\mathbf{x},t)$ is clearly a highly fluctuating function of space and time resulting in the need for much temporal and spatial averaging to obtain accurate velocity or pressure fields. To eliminate the need for this averaging, as well as gain insight into the FHP lattice gas, a lattice Boltzmann model can be constructed. A lattice Boltzmann model follows from the Boltzmann approximation that particles are uncorrelated. One may then construct a model based on the mean particle populations instead of the discrete particles.[14,15] Statistical fluctuations are then nonexistent.

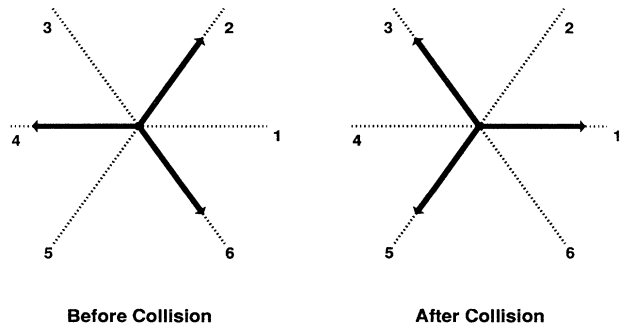

FIG. 1. An example of a three-particle collision in the FHP model. The particles collide and rotate by 60°. The numbers refer to the labeling of the lattice directions.

The collisions in a lattice Boltzmann model can be performed in two ways. In the first method, the collisions are straightforward analogs of the FHP particle collisions.[14] The Boolean variables $n_i(\mathbf{x},t)$ are replaced by the average population densities $N_i(\mathbf{x},t)$ and the logical operations in the collision operator replaced by their floating-point equivalents. For example, the lattice Boltzmann equivalent of the collision of Eq. (2) is

$$\Delta_1(N)=N_2N_4N_6(1-N_1)(1-N_3)(1-N_5)\ , \tag{3}$$

where $0\le N_i\le 1$ is the mean population density of lattice direction i. All of the other FHP collisions have a similar Boltzmann representation.

By writing all of the FHP collisions in their Boltzmann form and performing propagation of the mean populations in the same manner as propagation of the particles, a lattice Boltzmann model that is the floating-point counterpart of the discrete FHP model can be constructed. Equations close to the incompressible Navier-Stokes equations can be recovered for the Boltzmann model in exactly the same fashion as for the FHP model.

For small departures from equilibrium, this Boltzmann model can be simplified by linearizing the collision operator about the local equilibrium distribution.[15,16] From now on we will consider a model in two space dimensions with additional rest particles, where N_0 is the average population density of rest particles. We can write the time evolution of this lattice Boltzmann system as

$$N_i(\mathbf{x}+\mathbf{c}_i,t+1)=N_i(\mathbf{x},t)+\sum_{j=0}^{6}\Omega_{ij}N_j^{\mathrm{neq}}(\mathbf{x},t)\ , \tag{4}$$

where Ω_{ij} is the linearized collision operator described below and N_i^{neq} is the nonequilibrium part of the probability distribution. N_i^{neq} is given by

$$N_i^{\mathrm{neq}}=N_i-N_i^{\mathrm{eq}}\ , \tag{5}$$

where N_i^{eq} is the equilibrium distribution up to second order in velocity. For a site with average population density of $d=(M_cN_0+\sum_{i=1}^{6}N_i)/(6+M_c)$ in each direction, and velocity $\mathbf{v}=\sum_{i=1}^{6}N_i\mathbf{c}_i/d(6+M_c)$, the equilibrium distribution N_i^{eq} for a model with a maximum of M_c rest particles is given by a pseudo-Fermi-Dirac-distribution

$$N_i^{\mathrm{eq}}=d_0\left[1+\frac{\Delta d}{d_0}+2c_{i\alpha}v_\alpha+G(d_0)Q_{i\alpha\beta}v_\alpha v_\beta\right]\ , \tag{6}$$

where d_0 is the average population density on the lattice, $\Delta d=d-d_0$ and

$$G(d_0)=\frac{6+M_c}{3}\frac{1-2d_0}{1-d_0}\ ,$$
$$Q_{i\alpha\beta}=c_{i\alpha}c_{i\beta}-\tfrac{1}{2}\delta_{\alpha\beta}\ . \tag{7}$$

These equations are similar to the equilibrium equations discussed in Ref. 3 but modified here for the inclusion of M_c rest particles. Following Ref. 17, Galilean invariance is restored to the model by setting the maximum number of rest particles to

$$M_c=\frac{12(1-d_0)}{1-2d_0}-6 . \tag{8}$$

We note that a different equilibrium distribution which would not require the addition of rest particles to achieve Galilean invariance could be used instead of the distribution of Eq. (6). However, as described later, we require at least one rest particle in order to ensure that the interfaces remain as thin as possible. Since the computational cost of adding M_c rest particles is the same as adding one, we have chosen to use the equilibrium distribution found for the discrete lattice-gas models, thus maintaining a close connection to the discrete models.

The linearized collision operator Ω is constructed in the following fashion. Following Ref. 16, we note that since Ω is rotationally invariant, then for $1\le i,j\le 6$, we may write $\Omega_{ij}=\Omega_{|i-j|}$. We therefore denote Ω_{ij} by a_0, a_{60}, etc. for $1\le i,j\le 6$, where a_θ represents the collisions between moving particles on lattice links θ degrees apart. In addition to the collisions between moving particles there are collisions that create and destroy rest particles, given by probabilities b and c, respectively. The linearized collision operator is then given by

$$\Omega=\begin{bmatrix} c & \mathbf{b}^T \\ \mathbf{b} & \mathbf{A} \end{bmatrix} , \tag{9}$$

where $\mathbf{A}$ is a circulant matrix[18] with $(a_0,a_{60},a_{120},a_{180},a_{120},a_{60})$ as its top row and $\mathbf{b}=b(1,1,1,1,1,1)^T$. Ω has six unknown coefficients which must be computed. The eigenvalues and eigenvectors of Ω are computed using an extension of the theory of circulant matrices.[2] There are three zero eigenvalues with eigenvectors

$$\begin{aligned} \mathbf{x}_0&=(M_c,1,1,1,1,1,1)^T , \\ \mathbf{x}_1&=(0,2,1,-1,-2,-1,1)^T , \\ \mathbf{x}_2&=(0,0,1,1,0,-1,-1)^T , \end{aligned} \tag{10}$$

corresponding to conservation of mass and two components of momentum, respectively. For Ω to be nontrivial, these three conservation relations give the following equations:

$$\begin{aligned} &a_0+2a_{60}+2a_{120}+a_{180}+M_c b=0 , \\ &6b+M_c c=0 , \\ &a_0+a_{60}-a_{120}-a_{180}=0 . \end{aligned} \tag{11}$$

In addition we can specify the remaining nonzero eigenvalues,

$$\begin{aligned} \lambda&=6(a_0+a_{60})+2M_c b , \\ \gamma&=-6(a_0+2a_{60})-3M_c b , \\ \tau&=-\left[\frac{6}{M_c}+M_c\right]b . \end{aligned} \tag{12}$$

These eigenvalues represent the rate of decay of particular combinations of $N_i^{\rm neq}$ to the equilibrium configuration. For example, τ controls the rate at which rest particles equilibrate with the moving particles. λ is the most important eigenvalue as it determines the fluid's kinematic viscosity ν via the relation[3,16]

$$\nu=\frac{-1}{4}\left[\frac{1}{\lambda}+\frac{1}{2}\right] . \tag{13}$$

By lowering λ close to -2, we can lower ν arbitrarily close to zero, even if the corresponding matrix has no particle-based equivalent. However, care must be taken to ensure that the smallest scale of the simulated flow is greater than the lattice scale or numerical inaccuracies will result. When combined with Eq. (11), Eq. (12) enables us to compute the values of the six components of Ω_{ij}. Since $N_i^{\rm neq}$ decays like $1+\lambda$, $1+\gamma$, or $1+\tau$, we normally set γ and τ to be equal to -1 so that $N_i^{\rm neq}$ decays to zero as quickly as possible and use λ to set the kinematic viscosity.

LATTICE BOLTZMANN OPERATOR FOR IMMISCIBLE FLUIDS

In the immiscible lattice-gas (ILG) model of Ref. 8, the particles are colored either red or blue and the collision rules are modified to obtain surface tension between the two fluids. Essentially, these collision rules optimally send particles of one color to neighboring sites containing other particles of the same color.

Our lattice Boltzmann model of immiscible fluids is both a variant of the ILG and an extension of the Boltzmann formulation of the previous section. As in the ILG, the mass is colored either red or blue and the collisions are modified to obtain surface tension between the two fluids. However, our collision operator for producing surface tension is substantially different than the one used in the ILG. Specifically, we have designed a two-step two-phase collision rule. The first step of the two-phase collision is to add a perturbation to the particle distribution near an interface which creates the correct surface-tension dynamics. In the second step we recolor the mass to achieve zero diffusivity of one color into the other.

The immiscible lattice Boltzmann algorithm can be summarized as follows.

(1) Single-phase collision. (a) Compute $N_i=R_i+B_i$. (b) Compute d, $\mathbf{v}$, and $N_i^{\rm neq}$ from N_i. (c) Perform a single-phase collision obtaining $N_i'=N_i+\sum_{j=0}^{6}\Omega_{ij}N_j^{\rm neq}$.

(2) Two-phase collision. (a) Add a surface-tension inducing perturbation to N_i' obtaining N_i'' [Eq. (17)]. (b) Recolor the N_i'' to obtain R_i'' and B_i'' [Eq. (18)].

(3) Propagate the R_i'' and B_i'' according to

$$R_i(\mathbf{x}+\mathbf{c}_i,t+1)=R_i''(\mathbf{x},t)\ ,$$
$$B_i(\mathbf{x}+\mathbf{c}_i,t+1)=B_i''(\mathbf{x},t)\ . \tag{14}$$

The single-phase collision (step 1) has been described in the previous section. We discuss the two-phase collision (step 2) in detail below.

We note in passing that if a zero-surface-tension, zero-diffusivity model is desired then the first part of the two-phase collision [step 2(a)] can be omitted. The model will then track passive interfaces between fluids. We return to this point later.

Two-phase collision rule: Perturbation step

The first step of the two-phase collision rule is to add an anisotropic perturbation to the particle distributions near an interface. An interface is located by examining the magnitude of the local color gradient,

$$\mathbf{f}(\mathbf{x})=\sum_{i=1}^{6}\mathbf{c}_i\left[M_c[R_0(\mathbf{x}+\mathbf{c}_i)-B_0(\mathbf{x}+\mathbf{c}_i)]+\sum_{j=1}^{6}[R_j(\mathbf{x}+\mathbf{c}_i)-B_j(\mathbf{x}+\mathbf{c}_i)]\right], \tag{15}$$

where R_i and B_i indicate the amount of red and blue mass with velocity $\mathbf{c}_i$ present at a site. Note that $|\mathbf{f}|$ is large near an interface between two fluids and small in a homogeneous region. In addition we define $\theta_f=\tan^{-1}(f_y/f_x)$ as the angle of the local color gradient and note that the gradient is perpendicular to an interface. We set $N_i=R_i+B_i$, and apply the linearized collision operator of the previous section to N_i to obtain

$$N_i'=N_i+\sum_{j=0}^{6}\Omega_{ij}N_i^{\mathrm{neq}}\ . \tag{16}$$

Then, at sites where $|\mathbf{f}|>\epsilon$, where ϵ is a small number, we add a perturbation to N_i' such that

$$N_i''=N_i'+A|\mathbf{f}|\cos2(\theta_i-\theta_f)\equiv N_i'+C_i^b\ , \tag{17}$$

where $\theta_i=(i-1)\pi/3$ is the angle of lattice direction i and C_i^b is our surface-tension inducing binary-fluid perturbation. The binary-fluid collision operator C_i^b redistributes mass near an interface, depleting mass along lattice links parallel to an interface and adding mass to lattice links perpendicular to the interface, while conserving the total mass and the total momentum at the site. Here A is an arbitrary constant chosen to set the surface tension for the model.

Two-phase collision rule: Recoloring step

The second step in the collision rule is to recolor the mass after it has been perturbed in step 2(a). The outcome of recoloring is given by the solution to the maximization problem

$$W(\mathbf{R}',\mathbf{B}')=\max_{\mathbf{R}'',\mathbf{B}''}\left[\sum_{i=1}^{6}(R_i''-B_i'')\mathbf{c}_i\right]\cdot\mathbf{f} \tag{18}$$

subject to the following constraints:

$$M_cR_0+\sum_{i=1}^{6}R_i''=R_T\ ,$$
$$R_i''+B_i''=N_i''\ , \tag{19}$$

where R_T is the total amount of red mass present at the site before collision. These rules conserve the total amount of red mass, the total amount of blue mass, and the mass in each lattice direction.

We note that the inclusion of rest particles (i.e., $M_c>0$) allows interfaces to be only one lattice unit thick. The thin interfaces result because a site on an interface can react to a perturbation in the amount of mass of one color entering the site by altering the ratio of the red rest mass to the blue rest mass. However, if the model does not include rest particles then the site would be forced to send some mass of one color towards sites containing the other color and the interface thickness would increase.

Analysis of collision rule

An analysis of the collision rule hinges only on step 2(a) since this is when the model dynamics are perturbed. We recall the mechanical definition of the surface tension,

$$\sigma=\int_{-\infty}^{\infty}(P_N-P_T)dz\ , \tag{20}$$

where P_N and P_T are the normal pressure and the tangential pressure, respectively, in the neighborhood of an interface, and the integral is evaluated in a direction perpendicular to the interface.[19] This geometry is shown in Fig. 2, where z is the direction perpendicular to the interface, w is the direction parallel to the interface, and x and y are the usual Cartesian coordinates with x lying along a lattice line. We denote the angle between the x and z axes as $\bar{\theta}_f$.

The pressure tensor for a two-dimensional lattice gas is

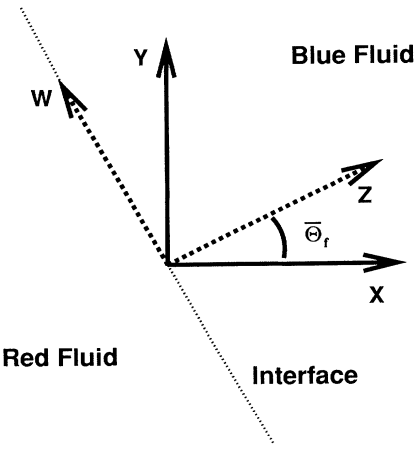

FIG. 2. Interface geometry for collision rule analysis. z is the axis perpendicular to the fluid-fluid interface, w is parallel to the interface, and x and y are the usual Cartesian coordinate axes. The lattice is oriented such that the 1 and 4 directions lie on the x axis.

given by[3]

$$P_{\alpha\beta}=\sum N_i c_{i\alpha}c_{i\beta} , \tag{21}$$

which yields

$$\begin{aligned} P_N=P_{zz}&=\sum_{i=1}^{6} N_i c_{iz}c_{iz} , \\ P_T=P_{ww}&=\sum_{i=1}^{6} N_i c_{iw}c_{iw} , \end{aligned} \tag{22}$$

where c_{iz} and c_{iw} are the components of velocity $\mathbf{c}_i$ in directions z and w and are given explicitly by

$$\begin{aligned} c_{iz}&=\cos(\theta_i-\bar{\theta}_f) , \\ c_{iw}&=\sin(\theta_i-\bar{\theta}_f) . \end{aligned} \tag{23}$$

Using these definitions, converting the integral in Eq. (20) to a sum over all $\mathbf{x}$ on the lattice and adding a $\cos\bar{\theta}_f$ factor to account for the angle between the x and z axes we find

$$\sigma=\frac{\cos\bar{\theta}_f}{n_y}\sum_{\mathbf{x}}\sum_{i=1}^{6} N_i(\mathbf{x})(c_{iz}^2-c_{iw}^2) , \tag{24}$$

where we are averaging over n_y lines parallel to the x axis. We let $U_i=c_{iz}^2-c_{iw}^2$ and remark that to first order in $\mathbf{v}$,

$$\sum_i U_i N_i^{\mathrm{eq}}=0 \tag{25}$$

giving

$$\sigma=\frac{\cos\bar{\theta}_f}{n_y}\sum_{\mathbf{x}}\sum_{i=1}^{6} U_i N_i^{\mathrm{neq}}(\mathbf{x},t) . \tag{26}$$

Adding the surface-tension inducing perturbation (17) to the lattice Boltzmann evolution Eq. (4) and then summing both sides of the equation over the entire lattice, we obtain

$$\sum_{\mathbf{x}} N_i(\mathbf{x}+\mathbf{c}_i,t+1)=\sum_{\mathbf{x}}\left[N_i(\mathbf{x},t)+\sum_j \Omega_{ij}N_j^{\mathrm{neq}}(\mathbf{x},t)+C_i^b(\mathbf{x},t)\right] . \tag{27}$$

For a lattice at steady state with reasonable boundary conditions we have

$$\sum_{\mathbf{x}} N_i(\mathbf{x}+\mathbf{c}_i,t+1)=\sum_{\mathbf{x}} N_i(\mathbf{x},t) \tag{28}$$

giving

$$\sum_{\mathbf{x}}\left[\sum_j \Omega_{ij}N_j^{\mathrm{neq}}(\mathbf{x})+C_i^b(\mathbf{x})\right]=0 . \tag{29}$$

Since U_i is an eigenvector of Ω with eigenvalue λ we find from Eq. (29) that

$$\sum_{\mathbf{x}}\sum_i U_i N_i^{\mathrm{neq}}(\mathbf{x})=-\lambda^{-1}\sum_{\mathbf{x}}\sum_i U_i C_i^b(\mathbf{x}) . \tag{30}$$

Substituting this equation and Eq. (17) into Eq. (26) gives

$$\sigma=-(n_y\lambda)^{-1}(\cos\bar{\theta}_f)\times\sum_{\mathbf{x}}\sum_i U_i A|\mathbf{f}(\mathbf{x})|\cos[2(\theta_f-\theta_i)] , \tag{31}$$

where θ_f is the local gradient angle. Note that $\theta_f\neq\bar{\theta}_f$, the average gradient angle, in general except for $\theta_f=0°$ and 30° because the discrete lattice creates spatial fluctuations in θ_f.

In order to evaluate Eq. (31) we consider a box of fluid containing an interface with average gradient angle $\bar{\theta}_f$. We assume that the interface is thin and we have perfect separation of red and blue. In addition we assume a uniform distribution of mass on the lattice with $(6+M_c)d$ total mass at each site. The interface will be composed of segments of two different types, shown in Fig. 3 which have $\theta_f=0°$ and 30°, respectively. These two segments will occur with probability $1-\sqrt{3}\tan\bar{\theta}_f$ and $\sqrt{3}\tan\bar{\theta}_f$, respectively.

Computing σ for interface 1 by calculating the value of Eq. (31) we obtain

$$\sigma_1=-\lambda^{-1}(\cos\bar{\theta}_f)[18A(6+M_c)d\ \cos(2\bar{\theta}_f)] . \tag{32}$$

Interface 2 gives

$$\sigma_2=-\lambda^{-1}(\cos\bar{\theta}_f)[12\sqrt{3}A(6+M_c)d\ \cos(2\bar{\theta}_f-\pi/3)] . \tag{33}$$

Mixing the two cases, weighted by their probability of occurrence we obtain the following explicit formula for the surface tension, accurate to first order in velocity,

$$\sigma=-18\lambda^{-1}Ad(6+M_c)F(\bar{\theta}_f) , \tag{34}$$

where

$$F(\bar{\theta}_f)=2[\sin(\pi/6-\bar{\theta}_f)\cos(2\bar{\theta}_f)+\cos2(\pi/6-\bar{\theta}_f)\sin\bar{\theta}_f] . \tag{35}$$

We note that this formula has a 12-fold anisotropy with a maximum deviation of approximately 10% at $\bar{\theta}_f=\pi/12$.

A similar analysis can be carried out if we instead assume that the interface is very wide with a slow variation

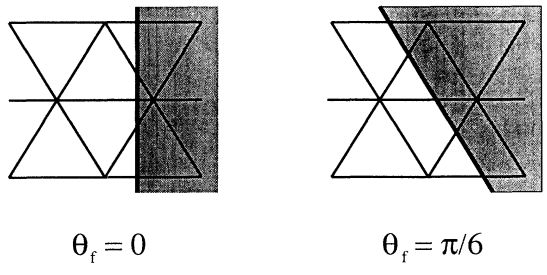

FIG. 3. The two types of interface segments which compose the interface are shown as 1 and 2. They have $\theta_f=0°$ and 30° and occur with probability $\sqrt{3}\tan\bar{\theta}_f$ and $1-\sqrt{3}\tan\bar{\theta}_f$, respectively.

of the color across the interface. Equation (34) is then recovered with $F=1$. The agreement between the two calculations indicates that surface tension is approximately independent of the actual distribution of color near the interface.

We note that if $A=0$, then σ will be zero as well. In this case only the second step of the collision procedure is performed, resulting in a model with zero surface tension and zero diffusivity. This model, a variant of the immiscible lattice Boltzmann model, has some potential applications in the study of complex flows involving passive interfaces.

SURFACE-TENSION MEASUREMENTS

Three methods are employed to measure surface tension. The first of these computes the surface-tension coefficient from Eq. (20), while the second employs a bubble test[17] to verify Laplace's law of surface tension. In addition a dynamic test of the surface tension was performed by measuring oscillations of a capillary wave.

Mechanical surface-tension measurements

This test is essentially a numerical evaluation of Eq. (20), the mechanical definition of surface tension. A lattice 256 units long by 16 units wide was initialized with an interface in the center of the lattice and allowed to evolve to steady state. The difference between P_N and P_T is then calculated and summed along a line perpendicular to the interface, giving the value of σ.

The surface tension was measured with this method for two orientations of the interface, $\bar{\theta}_f=0°$ and $\bar{\theta}_f=30°$. The results of these tests for a range of particle densities is shown in Fig. 4. The points represent the values measured in the simulations and the line shows the theoretical prediction from Eq. (34). The measurements in both directions agree very well with the theoretical prediction.

Bubble-test measurements

A second measurement of the surface tension was performed with a bubble test.[17] For a two-dimensional bubble at rest, Laplace's law states that

$$P_{\text{inner}}-P_{\text{outer}}=\frac{\sigma}{R}\ , \tag{36}$$

where P_{inner} and P_{outer} are the pressures inside and outside of the bubble, respectively, σ is the surface-tension coefficient, and R is the bubble radius.

The lattice was initialized with a bubble of one fluid in a sea of the other fluid. The pressure inside the bubble was measured by averaging the pressure at all sites inside a circle of radius $0.7R$ centered on the bubble and the outside pressure was measured by averaging the pressure at all sites more that $1.3R$ from the center of the bubble.

A number of tests with bubble radii ranging from 8 to 64 lattice units were run; the results are shown in Fig. 5. The values measured by simulations are shown as points while the theoretical values from Eqs. (34) and (36) are shown as a line. The linearity of the measured points in the plot shows that the correct scaling behavior of pressure difference with radius is present in the model. Moreover, the good fit of the measured points to their theoretical values indicates that the model is behaving closely to our predictions.

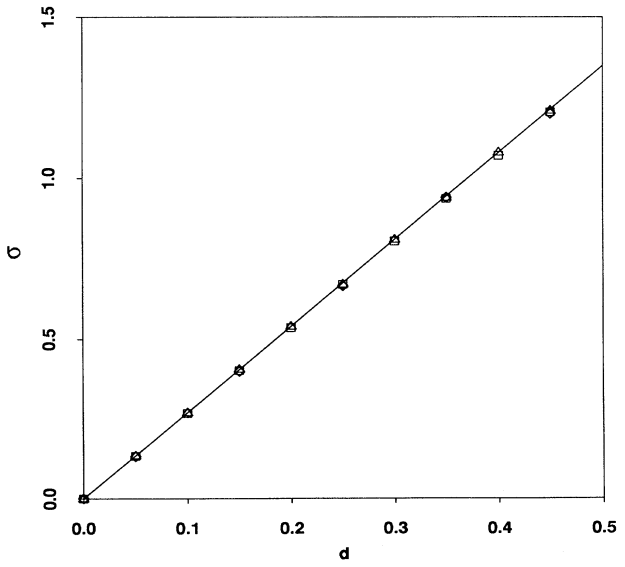

FIG. 4. The results of mechanical surface-tension measurements. Values measured in simulations are shown as points (squares for $\bar{\theta}_f=0°$ and triangles for $\bar{\theta}_f=30°$) and the theoretical prediction is shown as a solid line. The measured points and the prediction agree quite closely.

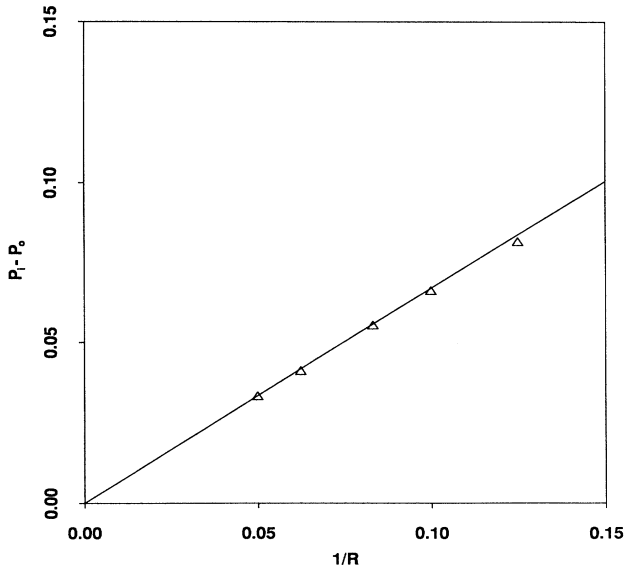

FIG. 5. The results of the bubble-test measurements of surface tension showing ΔP vs $1/R$. The measured values are plotted as triangles and the theoretical prediction is shown as a solid line. Again the agreement between simulation and theory is quite close. Error bars are smaller than the size of the points used to plot the measurements.

Capillary-wave test

In order to test the surface-tension dynamics, a capillary-wave test was performed. The tests were performed on a lattice of height $2h$ with no-slip boundaries at the top and bottom of the box and periodic boundaries in the other direction. The oscillation of a capillary wave of wave number k and amplitude A at an interface in the middle of such a box of height will be of the form

$$z(x,t)=Ae^{i(\omega t+kx)}, \tag{37}$$

where ω satisfies[20]

$$\omega^2=\frac{k^3\sigma\ \tanh(kh)}{2\rho}, \tag{38}$$

where ρ is the fluid density.

The lattice was initialized with a capillary wave of low amplitude (relative to h) and allowed to relax to equilibrium, exhibiting oscillatory motion. The position of the interface, $z(x,t)$, was measured at each time step and the oscillation frequency found by Fourier-transforming $z(x_0,t)$ over time at some x_0 and then choosing the frequency with maximum amplitude as the oscillation frequency.

Wavelengths ranging from 16 to 128 lattice units were tested. Figure 6 shows the comparison between the theoretical prediction of the dispersion relation and the measured values. The two curves match closely indicating that the model is correctly simulating surface-tension effects in a dynamic system as well as a static system.

TWO-PHASE FLOW IN POROUS MEDIA

As an example of a preliminary application of our model we show a simulation of two-phase flow in a microscopic model of a porous medium. Since lattice-gas and lattice Boltzmann methods can easily incorporate solid boundaries of arbitrary geometric complexity, flow through porous media is one of the most promising applications of these new methods.

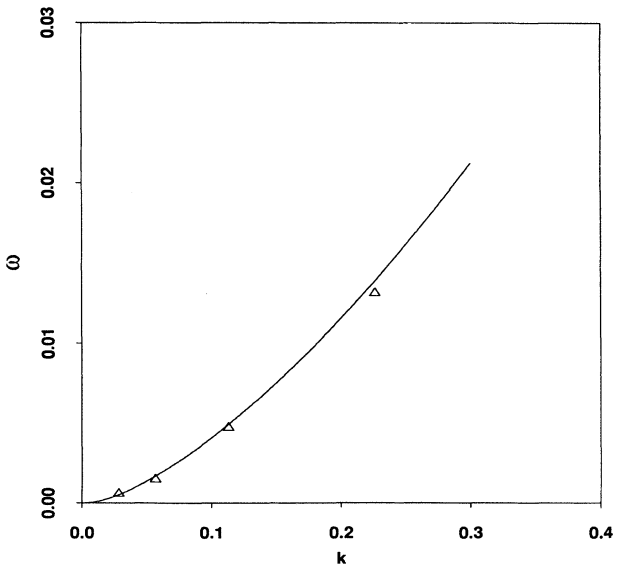

FIG. 6. The capillary-wave dispersion relationship is plotted. Values measured from simulations are shown as points and predictions from linear theory as a solid line. The measured points agree fairly well with the theoretical predictions.

The microscopic model of a porous medium used in the simulation is similar to that used by Lenormand, Zarcone, and Sarr in laboratory experiments.[21] The porous medium consists of randomly sized squares of solid material placed on a regular grid. No-slip boundary conditions are applied by using the "bounce-back" boundary conditions at solid sites.[22] A pressure difference is applied across the lattice by adding a fixed amount of momentum to the sites at one side of the lattice. The wetting properties of the solid matrix can be set by allowing the solid sites to bias the local color field.

For the simulation shown, the lattice is 108 lattice units wide and 80 lattice units long. The size of the squares in the model of the porous medium varies from 4 to 12 lattice units and the minimum channel width between two adjacent squares is 6 lattice units. The wetting properties are set such that the initially resident red fluid perfectly wets the solid matrix relative to the invading blue fluid. The pressure difference used in the simulation is chosen such that the invading fluid is not able to penetrate the narrow channels due to capillary effects. The capillary number for the simulation is approximately 10^{-2}.

Figure 7 shows the time evolution of the simulation. In the plot the invading blue fluid is shown as black, the resident red fluid as white and the solid matrix as grey. As expected the invading fluid is unable to penetrate the narrower channels, resulting in trapping of some of the resident fluid in these channels.

It is interesting to note that there are considerably more instances when the invading fluid does not penetrate into narrow or mid-sized channels than there would be in the equivalent simulation using the discrete ILG model. In ILG simulations of flow through porous media, random fluctuations of interfaces can be comparable to the size of small pores. However, when real fluids flow through real porous media, these fluctuations, of order $(kT/\sigma)^{1/2}$, are usually much smaller than the smallest pore size of interest. Thus the lattice Boltzmann model, which has no fluctuations, may be considered a more realistic method of simulating flow through a microscopic model of a porous medium.

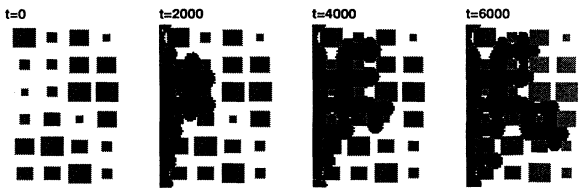

FIG. 7. The evolution of a two-phase flow in a microscopic model of a porous medium. The wetting, initially resident fluid is shown as white, the nonwetting, invading fluid as black, and the solid matrix as grey.

CONCLUSIONS

We have introduced a lattice Boltzmann model for the simulation of two immiscible fluids. The theoretical value of the surface-tension coefficient was derived. Simulations of bubbles and interfaces confirmed this prediction for fluids at rest and simulations of capillary waves verified this prediction for fluids in motion.

This model should be useful for gaining a better understanding of similar discrete models as well as for numerical studies of immiscible two-phase flow. Because flows through complex geometries may be easily simulated, the model is particularly promising for studies of flow through microscopic models of porous media. One such preliminary application has been demonstrated.

Compared to the immiscible lattice-gas model of Ref. 8, extensions of this lattice Boltzmann model to three dimensions are straightforward. Moreover, the lack of fluctuations in the lattice Boltzmann model obviates the need for spatial averaging in the determination of velocity fields. We note, however, that in our implementations, a single-site update of the ILG is approximately 10 times faster than in the lattice Boltzmann method. We can report one comparison with a finite-difference method. Simulations of capillary waves performed using the volume-of-fluid method of Hirt and Nichols[23] revealed an accuracy and efficiency similar to that obtained with the lattice Boltzmann model.

Extensions of our model to three dimensions are currently in progress. Subsequent work with the three-dimensional lattice Boltzmann model will then serve to better delineate the strengths and weaknesses of this new approach to the simulation of immiscible two-phase flow.

ACKNOWLEDGMENTS

This work was supported by National Science Foundation Grant No. EAR-8817027, NATO travel Grant No. 891061, and by the sponsors of the MIT Porous Flow Project. A.K.G, D.H.R., and G.Z. are also grateful to the Laboratoire de Physique Statistique, Centre National de la Recherche (CNRS), for financial support and hospitality during visits. Laboratorie de Physique Statistique de l'Ecole Normale Supérieure is associated with CNRS, as well as Universities of Paris 6 and 7. A.K.G. thanks Denis Mustafa for many interesting discussions.

[1]U. Frisch, B. Hasslacher, and Y. Pomeau, Phys. Rev. Lett. **56**, 1505 (1986).

[2]S. Wolfram, J. Stat. Phys. **45**, 471 (1986).

[3]U. Frisch, D. d'Humières, B. Hasslacher, P. Lallemand, Y. Pomeau, and J. -P. Rivet, Complex Systems **1**, 648 (1987).

[4]L. Kadanoff, G. McNamara, and G. Zanetti, Phys. Rev. A **40**, 4527 (1989).

[5]G. Zanetti, Phys. Rev. A **40**, 1539 (1989).

[6]J. -P. Rivet, M. Hénon, U. Frisch, and D. d'Humières, Europhys. Lett. **7** (3), 231 (1988).

[7]D. H. Rothman, Geophysics **53**, 509 (1988).

[8]D. H. Rothman and J. Keller, J. Stat. Phys. **52**, 1119 (1988).

[9]C. Appert and S. Zaleski, Phys. Rev. Lett. **64**, 1 (1990).

[10]A. K. Gunstensen and D. H. Rothman, Physica D **47**, 47 (1991).

[11]D. H. Rothman, J. Geophys. Res. **95**, 8663 (1990).

[12]M. Hénon, in *Discrete Kinetic Theory, Lattice-Gas Dynamics, and Foundations of Hydrodynamics,* edited by R. Monaco (World Scientific, Singapore, 1989), p. 146.

[13]P. Rem and J. Somers, in *Discrete Kinetic Theory, Lattice-Gas Dynamics, and Foundations of Hydrodynamics,* (Ref. 12), p. 268.

[14]G. McNamara and G. Zanetti, Phys. Rev. Lett. **61**, 2332 (1988).

[15]F. Higuera and J. Jimenez, Europhys. Lett. **9** (7), 663 (1989).

[16]F. Higuera, S. Succi, and R. Benzi, Europhys. Lett. **9** (4), 345 (1989).

[17]A. K. Gunstensen and D. H. Rothman, Physica D **47**, 53 (1991).

[18]P. J. Davis, *Circulant Matrices* (Wiley, New York, 1979).

[19]J. Rowlinson and B. Widom, *Molecular Theory of Capillarity* (Clarendon, Oxford, 1982).

[20]S. Chandrasekhar, *Hydrodynamic and Hydromagnetic Stability* (Oxford University Press, Oxford, 1961).

[21]R. Lenormand, C. Zarcone, and A. Sarr, J. Fluid Mech. **135**, 337 (1983).

[22]R. Cournubert, D. d'Humiéres, and D. Levermore, Physica D **47**, 241 (1991).

[23]C. W. Hirt and B. D. Nichols, J. Comp. Phys. **39**, 201 (1981).